Far-infrared studies of the phase transition and conduction mechanism in the fast-ion conductors Ag_2HgI_4 and Cu_2HgI_4

H. G. LeDuc* and L. B. Coleman
Department of Physics, University of California at Davis, Davis, California 95616
(Received 16 July 1984)

A study of the temperature dependence of the far-infrared reflectance of the fast-ion conductors Ag_2HgI_4 and Cu_2HgI_4 has been completed. These materials are unusual in that the transition into the fast-ion conducting state is first order with a disordering of several cation species, but no reconstitution or symmetry change of the "rigid" anion sublattice. By examining the temperature dependence of the phonon lifetimes, we find that the phase transition into the fast-ion state occurs more rapidly than in typical fast-ion materials such as AgI. In addition, the low-frequency modes are strongly anharmonic and tightly coupled to the mobile ions. We conclude that the existence of three disordering ion species (monovalent silver or copper ions, divalent mercury ions, and vacancies) leads to a two-component disordering, where the mercury ions act to block the monovalent cation and vacancy disordering.

I. INTRODUCTION

Interest in the phenomenon of fast-ion transport in solids has grown rapidly over the past decade.[1] Fast-ion conductors (also referred to as superionic conductors or solid electrolytes) are of continuing interest not only for their high ionic mobilities and technological promise, but also as solid-state systems for the study of a wide range of problems. Research in the areas of ionic diffusion, molecular dynamics, lattice dynamics, nonstoichiometric, disordered, and amorphous solids, and phase transitions have been successfully carried out using fast-ion conductors and a wide range of experimental and theoretical techniques. While these materials are linked by their high ionic conductivities, they display a wide variety of behavior in both the critical region and in the fast-ion state. It is unlikely that a single theoretical model will adequately describe these systems, and this adds to the interest in them.

We have examined the far-infrared response of two ternary compounds, Ag_2HgI_4 and Cu_2HgI_4. Our primary interest in these compounds is their unique phase transition. Both of these materials undergo a first-order phase transition into the fast-ion state at relatively low temperatures (323 K for Ag_2HgI_4 and 340 K for Cu_2HgI_4, compared to 420 K for AgI), as noted by a sharp discontinuity in the ionic conductivity. However, unlike the majority of materials displaying this type of fast-ion transition, for example AgI, the phase transition in these materials is totally cation order-disorder with no reconstitution of the anion sublattice. This phase transition is very rapid and shows no precursory behavior until just below the transition temperature. From an examination of the far-infrared reflectance of these materials from 100 K to above their phase transition temperatures, we are able to follow the dynamics of the phase transition and to model the conduction mechanism.

II. CRYSTAL STRUCTURE AND SELECTION RULES

The crystal structures of Ag_2HgI_4 and Cu_2HgI_4 have been determined by several authors.[2–5] Ketelaar, in his pioneering papers,[2] proposed a pseudocubic space group $P42m$ for the low-temperature β phase of both materials and a high-temperature α phase in which the iodine lattice retains its symmetry and the cation and vacant lattice sites become randomly occupied (by either a cation or a vacancy). Later studies[3,5] showed that the low-temperature phases are tetragonal and in addition, are not isostructural, differing in the placement of the two monovalent cations (Ag or Cu) and the vacancy (see Fig. 1). The space groups are $I\bar{4}$ and $I\bar{4}2m$ for Ag_2HgI_4 and Cu_2HgI_4, respectively. In the tetragonal structure both cations (Ag or Cu, and Hg) reside in sites which are tetrahedrally coordinated with respect to the rigid iodine lattice. As in Ketelaar's description, the α phase retains the same iodine structure as in the β phase, while the cation and vacancy sites become equivalent. Another way

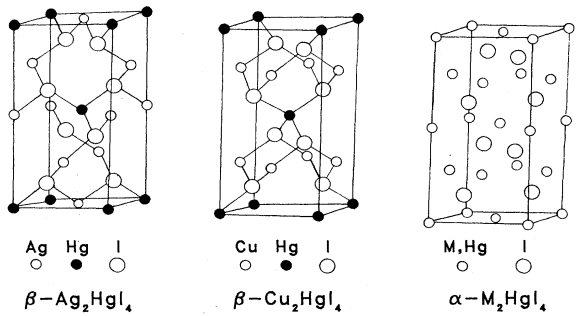

FIG. 1. Crystal structures of β-Ag_2HgI_4, β-Cu_2HgI_4, and α-M_2HgI_4, with M = Ag or Cu.

to view these crystal structures is as ordered-vacancy chalcopyrites[6] whose chemical formulas would be $Ag_2Hg\square I_4$ and $Cu_2Hg\square I_4$. The vacancies in the silver structure are occupied by the copper ions in the copper structure and vice versa. In the fast-ion conducting α phase all cations are distributed among the cation and vacancy sites, and the salts are isostructural.

There has been some controversy as to the nature of the most stable low-temperature phase or phases. Olsen and Harris,[4] from single-crystal x-ray studies, proposed that the tetragonal phase of Ag_2HgI_4 is only metastable for temperatures below the phase transition and after cycling through the transition the crystal relaxes into a stable cubic phase. Raman scattering, transport, and specific heat studies have shown the existence of a variety of phases of these materials above ambient pressure.[7–11] However, at room temperature the first phase boundary in Ag_2HgI_4 appears at 3.3 kbar and at 8.0 kbar in Cu_2HgI_4.[8]

Recently Browal *et al.*[5] carried out an exhaustive structural analysis on single crystals of Ag_2HgI_4 and found that their results depended on the quality and method of preparation of the crystals. They concluded, based on data from the best single crystals, that the tetragonal phase was the only stable low-temperature phase and the apparent phase change after cycling could be explained by the formation of domains with the tetragonal c axis randomly oriented along the three spatial axes, thus giving the impression of a cubic lattice. The interpretation of a single low-temperature phase has the broadest base of support of the two views at present.

Assuming the β phase is tetragonal, the number and symmetry of normal modes can be determined. Group-theory analysis finds the following numbers and symmetries for the 18 optical modes in each material:

$$Ag_2HgI_4: \ 3A+5B+5E \ ,$$

$$Cu_2HgI_4: \ 2A_1+A_2+2B_1+3B_2+5E \ .$$

The infrared and Raman selection rules give the following allowed-mode symmetries.

	Infrared	Raman
Ag	$5B+5E$ (10 bands)	$3A+5B+5E$ (13 bands)
Cu	$3B_2+5E$ (8 bands)	$2A_1+2B_1+3B_2+5E$ (12 bands)

Using projection operators, we find that the B symmetry modes involve motion of the cation along the tetragonal c axis (z), and the E modes involve motion of the cations along the a or b axes (x or y). For infrared processes, B modes couple to electric fields along the z axis and E modes couple to fields in the xy plane, so that polarized spectra would determine the mode-symmetry assignments uniquely. Unfortunately we were unable to grow single crystals of sufficient size to measure polarized spectra. However, Raman spectra are available for both materials,[8,11–14] and since, for these materials, all infrared-active modes are also Raman active, some symmetry assignments have already been made.

III. EXPERIMENTAL DETAILS

The samples used were polycrystalline compacted pellets prepared from material supplied by Ryan Dupon of Northwestern University and produced as in Ref. 15. Care must be taken in preparing and handling the samples for optical studies as both materials can be easily modified. Both salts decompose before melting and are subject to HgI_2 loss from vaporization at elevated temperatures and at low pressures. HgI_2 may also be leached out of the sample by a variety of organic solvents, and at elevated temperatures the samples will react with metals (particularly copper and silver). The silver material is mildly light sensitive and the copper material is somewhat hygroscopic. In addition they can be easily decomposed by a too rapid application of high pressures. The powders were pressed into a pellet $\frac{7}{16}$ in. in diameter in a stainless-steel die with lapped surfaces. To avoid phase changes and component separation, the pressure was increased in (2.3×10^6)-N/m^2 increments, waiting at least 30 s between each increment, to a final pressure of 2.3×10^7 N/m^2. When necessary, the sample surfaces were polished in stages starting with no. 600 grit paper, then several sizes of alumina polishing powders, and finally $\frac{1}{4}$-μm diamond powder and lens paper. This procedure resulted in a pellet whose surface reproducibly produced spectra of the bulk material.

Temperatures above room temperature were obtained using an Ohmic heated hot finger, while temperatures from ambient to 100 K were achieved with a continuous-transfer liquid-nitrogen cold finger. Calibrated thin-film platinum resistance thermometers[16] and electronic temperature control[17] were used. The sample mounts and holders were designed to eliminate stray light reflected from the sample mounting or transmitted by the sample from reaching the exit optics. To ensure good thermal contact and reliable thermometry the sample pellets were attached to annular copper forms with a high thermal conductivity, silica-filled epoxy.[18] Care was taken to avoid direct contact between the samples and the copper mounts. For temperature-dependent measurements, type-T (copper-Constantan) thermocouples were bonded to the back side of the samples with epoxy. These thermocouples gave an estimate of the front surface temperature for monitoring purposes during the data run. Direct temperature calibrations were made after the data were taken by bonding type-T thermocouples to the front surface of the sample. The absolute temperature was determined by a differential thermocouple with one junction mounted on the sample and the other on the platinum resistance thermometer in the heater block. When above room temperature, the sample was kept in an atmosphere of dry argon to avoid decomposition. After each run above or below room temperature, the room-temperature spectra were remeasured to check for damage to the sample surface.

Unpolarized reflectance spectra were measured at near-normal incidence in the range 6–4000 cm^{-1}. In the far infrared (6–400 cm^{-1}) a modified Beckman model FS 720 Michelson Interferometer was used. The interferometer was controlled by a Digital Equipment Corporation PDP 11/23 minicomputer which was also used for real time data acquisition and Fourier-transform analysis. Care was taken to filter out the intense visible and ultraviolet light from the mercury arc source before it

reached the sample. Two gallium-doped germanium composite bolometers[19] were used. One optimized for low frequency and low background radiation was operated at 1.7 K, and another optimized for higher frequency use was operated at 4.2 K. A combination of scatter and transmission low pass filters were mounted in the detector cryostat and cooled to either 1.7 or 4.2 K. Standard phase-sensitive detection techniques were used with an ultra-low noise preamplifier and lock-in amplifier input to an analog-to-digital converter. Additional noise reduction and spectral averaging as well as Fourier transformation and normalization were carried out in software. At room temperature the spectra were extended into the infrared (250—4000 cm^{-1}) using a Nicolet MX1-E fast-scan Fourier-transform spectrometer. Additional details of the experimental apparatus and sample preparation techniques have been reported elsewhere.[20]

IV. RESULTS

The far-infrared room-temperature compacted pellet reflectance of Ag_2HgI_4 and Cu_2HgI_4 are shown in Fig. 2. From 200 to 4000 cm^{-1} the reflectance of both materials was small ($<10\%$) and featureless. Transmission spectra taken at room temperature show that both materials become increasingly transparent below 20 cm^{-1}. This accounts for the apparent rise in reflectivity at the lowest frequencies shown, which we attribute to reflected power from the back surface. Above the phase transition the transmittance remains negligible throughout the far infrared. For both materials, the room-temperature reflectance spectra can be separated into two regions. Grieg *et al.*[13] observe the same separation in their Raman spectra and attribute the higher frequency bands to predominantly "bond-stretching" modes and the lower frequency modes to "bond bending."

We model the optical response of these materials using a sum of classical damped harmonic oscillators (Lorentzian modes). The frequency-dependent complex dielectric function (the response function responsible for the measured spectra) is then written as:[21]

$$\tilde{\epsilon}(\omega)=\epsilon_\infty+\sum_j \frac{f_j\omega_{0j}^2}{\omega^2-\omega_{0j}^2-i\gamma_j\omega}$$

$$=\epsilon_\infty+\sum_j \frac{S_j}{\omega^2-\omega_{0j}^2-i\gamma_j\omega}\ , \qquad (1)$$

where ϵ_∞ is the electronic part of the dielectric constant, f_j (or S_j) the oscillator strength,[22] ω_{0j} the mode frequency, and γ_j the damping coefficient.

The imaginary part of the dielectric constant is related to the real part of the conductivity as

$$\sigma_1(\omega)=\frac{\omega\epsilon_2(\omega)}{4\pi}\ . \qquad (2)$$

Normally the dielectric function is more easily visually interpreted than the reflectance. For small damping, the peaks of ϵ_2 occur at the transverse optical mode frequencies. The width of the modes at half maximum is the damping or inverse lifetime. Via the sum rules, the oscillator strength is proportional to the integrated conductivity. When damping becomes significant more care must be taken in obtaining the mode frequencies.

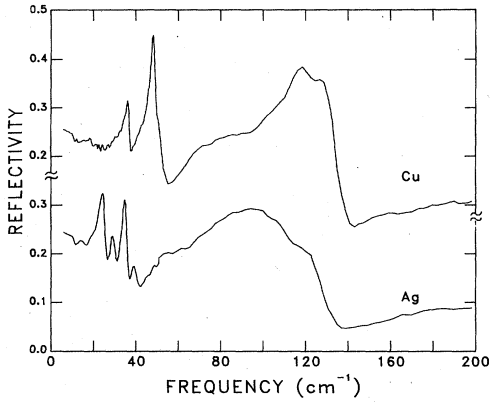

FIG. 2. Far-infrared room-temperature reflectivity of β-Ag_2HgI_4 and β-Cu_2HgI_4.

We obtain the complex dielectric function from the measured reflectance by using a Kramers-Kronig analysis.[23] This technique allows for the calculation of the frequency-dependent complex dielectric function from a knowledge of the reflectivity over all frequencies. Extrapolations are made for frequencies outside of the experimentally measured range. At high frequency, free-electron behavior is simulated and our low-frequency extrapolations were chosen to agree with the microwave dielectric constant and conductivity measurements of Wong and co-workers.[15,24] Below the phase transition the microwave dielectric function is nearly constant, while in the fast-ion state it rises below 0.25 cm^{-1}. Checks of various extrapolations to this data show little effect on our results above 10—15 cm^{-1}. Experience has shown

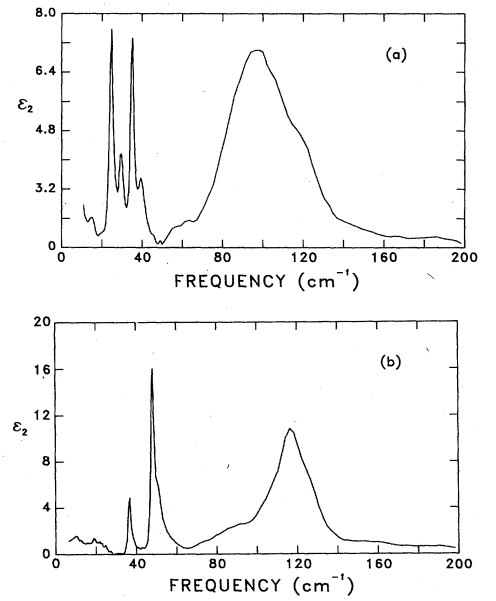

FIG. 3. The imaginary part of the room-temperature dielectric function [$\epsilon_2(\omega)$], determined by Kramers-Kronig analysis, versus frequency. (a), β-Ag_2HgI_4; (b), β-Cu_2HgI_4.

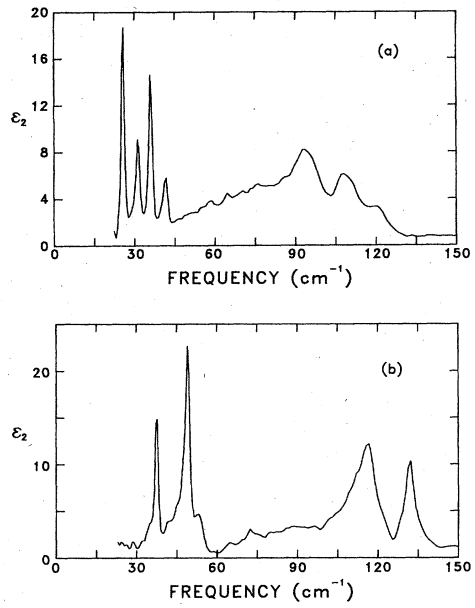

FIG. 4. The imaginary part of the dielectric function $[\epsilon_2(\omega)]$, determined by Kramers-Kronig analysis at 100 K, versus frequency. (a), β-Ag_2HgI_4; (b), β-Cu_2HgI_4.

that when the data extend over several decades or more in frequency and reasonable care is taken in the extrapolations, the Kramers-Kronig technique gives reliable and reproducible results. The resulting frequency dependence of the imaginary part of the dielectric functions (ϵ_2) is shown in Fig. 3.

The normal mode parameters (frequency, width, and oscillator strength) were obtained by fitting the imaginary part of the dielectric function to the Lorentzian oscillator model. This procedure has been found to be easier than a direct fit to the reflectivity because of the more direct interpretation of the fitting parameters in terms of structures in the imaginary part of the dielectric function. The parameters are then refined by a direct fit to the reflectivity, which assures against any deleterious effects of the extrapolations used in the Kramers-Kronig transformation.

Low-temperature reflectance spectra were obtained at 100 and 200 K, and ϵ_2 at 100 K is shown in Fig. 4. The 100-K spectra allow us to better resolve the modes in both spectral regions. The high-frequency region (80 to 140 cm^{-1}) contains three well-defined modes in the Ag_2HgI_4 spectrum and two in the Cu_2HgI_4 spectrum. The low-frequency regions contain four modes for the silver salt, and two well-defined modes and two shoulders appear in the copper material. The 100-, 200-, and 296-K mode frequencies obtained from the oscillator fits are listed in Tables I and II along with the reported Raman mode frequencies. For the copper sample, only the shoulder at 53.2 cm^{-1} is included since it persists at higher temperatures, while the other shoulder ($\sim$43 cm^{-1}) disappears. The far-infrared data from Joy[25] on Cu_2HgI_4 are also listed.

Wong and co-workers have observed a reproducible but transient peak in the microwave conductivity (at both 24 and 70 GHz) at or just before the phase transition.[15] Slowly heating through the phase transition, while monitoring the broad-band (15—75 cm^{-1}) reflected power, no similar unusual behavior was seen. At lower frequencies (below 20 cm^{-1}) a similar search of the transmittance was also uneventful. The sensitivity of our search would be limited by the efficiency of our spectrometer to above approximately 6—8 cm^{-1}.

V. DISCUSSION

Referring to Tables I and II, we see there is excellent agreement between our far-infrared results and the reported Raman modes. Without polarized single-crystal measurements, further symmetry assignments cannot be made precisely, however, some tentative assignments can be made from a consideration of the oscillator strengths of the observed modes. Modes of *B* symmetry are excited by electric fields along the *z* axis, while modes of *E* type respond to fields in the *xy* plane. For polycrystalline compactions and an unpolarized incident beam, one-third of the electric field is along any one of the Cartesian axes of microdomains. This implies that only one-third of the total number of oscillators along a given direction are excited. All other factors being equal, the doubly degenerate

TABLE I. Classical oscillator parameters for the far-infrared modes of β-Ag_2HgI_4 as a function of temperature. $\epsilon_\infty = 4.1$. Question marks indicate uncertain mode assignment.

Frequency ω_{to} (cm^{-1})			Oscillator strength f		Damping γ (cm^{-1})			ir mode	Raman mode	Raman mode
100 K	200 K	296 K	100 K	296 K	100 K	200 K	296 K	symmetry[a]	frequency[b]	symmetry[b]
25.2	24.9	24.8	1.06	0.55	1.6	1.7	2.0	*E*	24.4	*E*
31.4	30.3	29.8	0.48	0.20	1.6	2.4	2.5	*B*	29.3	*B*
35.8	35.2	35.1	0.55	0.37	1.6	1.7	1.8	*E*	34.7	*E*
41.0	40.3	39.5	0.12	0.12	3.2	3.4	3.0	*B*	40.0	*B*
									81.0	*A*
95.0	92.0	95.0	1.05	1.88	12.0	18.0	28.0	*B?E*	96[c]	?
110.0	110.0	108.0	0.47	0.24	9.0	14.0	15.5	*B?E*	106[c]	?
121.0	119.0	120.0	0.21	0.19	8.0	11.0	14.5	*B?E*	121[c]	?
									122	*A*

[a]Assignments based on oscillator strength arguments in this work.
[b]Some variation ($\pm$2—3 cm^{-1}) exists in the reported Raman frequencies. Data given are taken from Refs. 13 and 14.
[c]Observed only at low temperatures (182 and 8 K).

TABLE II. Classical oscillator parameters for the far-infrared modes of β-Cu_2HgI_4 as a function of temperature. $\epsilon_\infty = 5.1$. Question marks indicate uncertain mode assigment.

Frequency ω_{to} (cm^{-1})			Oscillator strength f		Damping γ (cm^{-1})			ir mode frequency	ir mode	Raman mode	Raman mode
100 K	200 K	296 K	100 K	296 K	100 K	200 K	296 K	from Joy[a]	symmetry[b]	frequency[c]	symmetry
37.5	36.8	36.8	0.64	0.22	1.5	2.0	1.7	35.8	E	37.0	E
49.0	48.3	48.0	0.77	0.59	1.3	1.4	2.0	40.1	E	48.0	$A_1?B_1$
53.2	52.0	51.3	0.28	0.38	4.0	5.0	4.8		B_2	53.0	?
								88.6		85	$A_1?B_1$
116.2	115.0	116.8	0.89	1.54	7.0	10.0	17.0	117.8	$B_2?E$	119	?
131.4	129.0	126.5	0.38	0.19	5.0	7.0	9.0	124.6	$B_2?E$	127	A_1

[a]From Ref. 25.

[b]Assignments based on oscillator strength arguments in this work.

[c]Some variation (± 2–3 cm^{-1}) exists in the reported Raman frequencies. Data given are taken from Refs. 13 and 14.

E modes would have twice the oscillator strength of the singlet B modes. Greig *et al.*[11] associate the low-frequency modes in their Raman data with metal halogen deformations, and from factor group analysis, point out there should be $2B+E$ Ag-I and $2B+E$ HgI_4 infrared-active deformation modes. It can be expected that the B- and E-type modes for each type of deformation have about the same coupling to the field. Therefore we expect this assumption (of all other factors being equal) to be valid for the low-frequency modes in both materials. In Ag_2HgI_4 the four lowest frequency modes support this assumption. The two lowest modes (Ag-I deformation) have strengths differing by approximately a factor of 2; similarly for the other two low-frequency modes (HgI_4 deformation modes). Using the same arguments for Cu_2HgI_4 we would assign the two strongest low-frequency modes (36.8 and 48 cm^{-1}) E symmetry and the weaker shoulder (53 cm^{-1}) B_2 symmetry. However, there is a discrepancy between these and the Raman mode assignments. The 48-cm^{-1} mode has been assigned either A_1 or B_1 symmetry, neither of which are infrared allowed. It is possible this assignment is correct and the infrared mode we see is degenerate or nearly degenerate with it. Raman spectra taken at 12 K show that the region between 53 and 48 cm^{-1} may contain as many as three modes, lending support to this hypothesis. Joy[25] observed a weak mode at 88.6 cm^{-1} which may correspond to a broad, poorly defined feature in our spectra at about the same frequency. The only Raman peak in that region is a fairly strong 85-cm^{-1} peak which is assigned (not very confidently) A_1 or B_1,[12] neither of which are infrared active. The high-frequency far-infrared modes have not been assigned symmetries, since they are very weak in the Raman spectra and are seen at low temperatures only. In contrast to the Raman spectra, the stretching modes in the infrared are strong (corresponding to the main reststrahlen bands in binary ionic salts); unfortunately, without polarized spectra no symmetries could be assigned.

The imaginary part of the dielectric function at room temperature (296 K), and at several temperatures near and on either side of the phase transition is shown in Figs. 5(a) (Ag_2HgI_4) and 5(b) (Cu_2HgI_4). The spectra of both materials exhibit the same qualitative behavior as the temperature is raised through the transition (323 K for Ag_2HgI_4 and 340 K for Cu_2HgI_4). All of the modes broaden dramatically and soften slightly. This behavior is

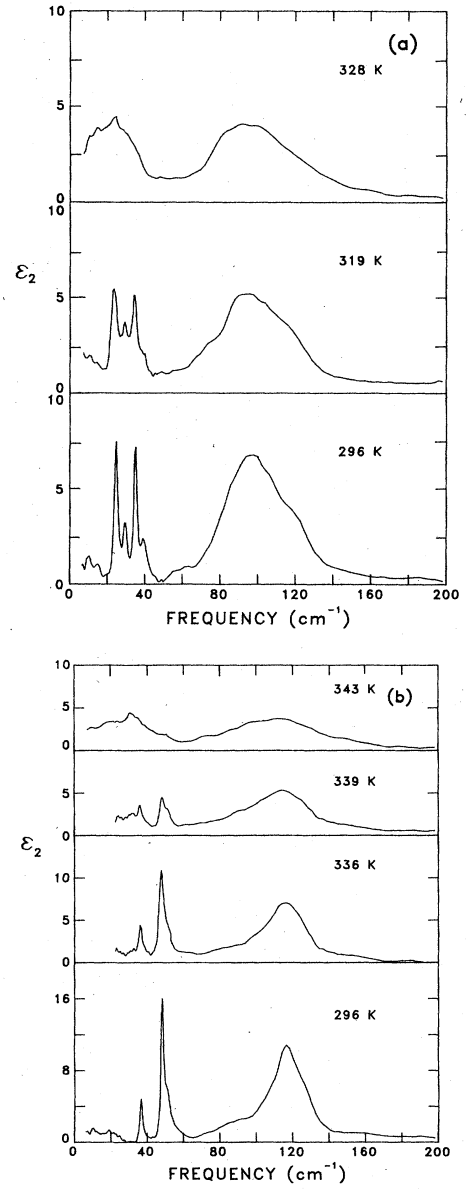

FIG. 5. The imaginary part of the dielectric function [$\epsilon_2(\omega)$] versus frequency at room temperature and at temperatures immediately below and above the phase transition. (a), Ag_2HgI_4, $T_c = 323$ K; (b), Cu_2HgI_4, $T_c = 340$ K.

common in fast-ion conductors where it is usually attributed to the disordering of the local environments and the decrease in phonon lifetimes associated with coupling to the mobile ions. Peyrard and Misset[26] observed the temperature dependence of the 108-cm^{-1} (Ag—I stretch) mode of AgI and proposed a simple model of its behavior. AgI exhibits a first-order phase transition (reconstitutive plus order-disorder) at 420 K in which it transforms discontinuously from a normal ionic conductor to a fast-ion conductor. For temperatures far below the transition temperature, the mode width varies linearly with temperature, indicating that cubic anharmonicity is the dominant phonon-decay process. With increasing temperature, the effects of the mobile silver cations on the mode width become apparent (even at temperatures 30 to 40 K below the transition temperature). Peyrard and Misset suggest the mode width is of the form

$$\gamma=\gamma_0+aT+b\sigma(0)$$

where γ_0, a, and b are constants to be determined by fitting the measured mode width and $\sigma(0)$ is the measured dc ionic conductivity. The first two terms represent the zero temperature width and the cubic anharmonicity and the last represents the coupling of the phonons to the mobile ions (the dc conductivity is assumed to be proportional to the concentration of mobile ions). Despite the simplifications in this model, good agreement with the measured mode widths in AgI was obtained.

There are several differences between AgI and M_2HgI_4 (M=Ag,Cu). One important difference is that the M_2HgI_4 materials remain ordered (in contrast to AgI) until very near the transition temperature, when rapid disordering occurs. Disordering in M_2HgI_4 involves two cations (M^+ and Hg^{2+}), as opposed to the single disordering species in AgI; and, as we will discuss below, this plays a significant role in the unique behavior of these materials. The temperature dependence of the measured stretching mode widths (equal to the inverse phonon lifetimes) for Ag_2HgI_4 is shown in Fig. 6. The copper sample exhibits similar behavior, but the overlapping of the modes results in large uncertainties in the fit-derived mode widths making quantitative analysis difficult. Above the phase transition, the modes in both materials

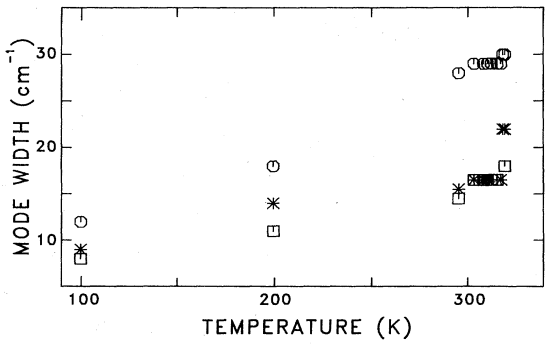

FIG. 6. Mode widths, determined by Lorentzian oscillator fits to the reflectance, versus temperature for Ag_2HgI_4 stretching modes. The room-temperature mode frequencies are as follows: ○, 95 cm^{-1}; ✱, 108 cm^{-1}; and □, 120 cm^{-1}.

are impossible to quantitatively resolve with any accuracy.

Below the transition temperature, the stretching mode widths are linearly increasing, consistent with cubic anharmonicity (see Fig. 6). This is in agreement with pressure-dependent Raman measurements[12] which show the Ag—I and Cu—I stretching modes exhibiting large anharmonicities. These modes are expected to involve both M—I and Hg—I bond stretching and the mode broadening is uniform. At first glance this observation appears to be at odds with the large difference in mobilities of the M and Hg ions (Ag is approximately 40 times more mobile than Hg), and the M—I stretching modes might be expected to broaden more than the Hg—I modes. Our results thus indicate strong coupling exists between these modes. Nitzan *et al.*[27] proposed a model describing the observed temperature-dependent line broadening of the stretching modes in the Raman spectra of compounds of the form M_2NX_4 (M=Ag,Cu,In,Tl,K; N=Hg,Zn; and X=Br,I). For M_2HgI_4 these modes occur at 122 and 82 cm^{-1} (Ag), and 127 and 85 cm^{-1} (Cu). The higher frequency mode is associated with a Hg—I stretch (or "breathing") mode and the lower with a M—I stretch mode. The large mobility difference suggests that the M—I stretch mode will have both oscillatory and diffusive character above the transition while the Hg—I mode will be mostly oscillatory. In the model, the dynamics of the M—I mode is described by a generalized Langenvin equation of motion and a memory function, while the dynamics of the Hg—I mode is described by a damped harmonic oscillator. The coupling between the modes is provided by another memory function which contains the correlation effects linking the mobile M^+ cations to the less mobile Hg^{2+}. The resulting calculated mode width agrees very well with the experimental values. Without a complete description of the dynamics of the stretching modes, we cannot extend this theory; however, the existence of a strong mode-coupling mechanism demonstrated by this model does give us some insight into the uniform broadening we have observed in this frequency range.

McOmber *et al.*[12,14] have assigned the lowest frequency infrared mode in each material to the attempt frequency (Ag, 24 cm^{-1}; Cu, 36 cm^{-1}). This assignment is based primarily on the scaling of these two modes with the inverse square root of the ion mass, indicative of a major contribution to these modes from the bare ions. However, the concept of an attempt frequency is poorly defined in these materials, particularly since the conduction path is likely to involve motion along all three axes (from one tetrahedral site through an octahedral site into another tetrahedral site). The cooperative motion needed for this type of motion again suggests that the modes become strongly coupled in the ionically conducting phase and possibly just below the transition temperature as well. Our results demonstrate that all of the low-frequency modes broaden together as the transition is approached, which confirms the strong coupling between modes suggested above.

The temperature dependence of the deformation mode widths in Ag_2HgI_4 is shown in Fig. 7. The phase transition involves no structural change other than the disorder-

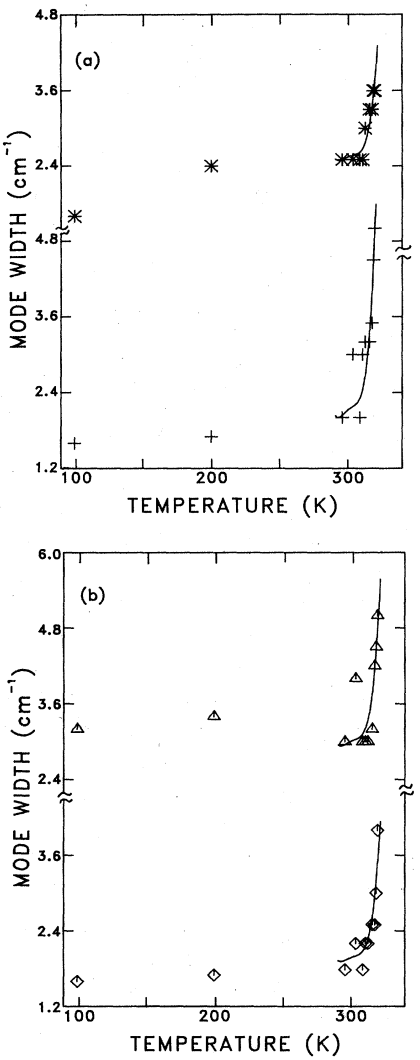

FIG. 7. Mode widths, determined by Lorentzian oscillator fits to the reflectance, versus temperature for Ag_2HgI deformation modes. The solid lines are from fits to $\gamma=\gamma_0+A\sigma(\mathrm{dc})$ in the phase-transition region. The room-temperature mode frequencies are as follows. (a): +, 24.8 cm^{-1}; *, 29.8 cm^{-1}. (b): ◇, 35.1 cm^{-1}, △, 39.5 cm^{-1}.

ing of the cations and an increase in the mobility of M^+ ions by approximately two orders of magnitude; therefore, the major contribution to the mode broadening is expected to come from lifetime effects associated with coupling of the phonons to the diffusing ions. In the case where coupling to the diffusing ions dominates, the mode width (or inverse lifetime) is proportional to the concentration of mobile cations. The exact form of the order parameter is not known for this phase transition; however, it is expected to be a function of the mobile cation concentration. Since the dc conductivity is also proportional to the concentration of mobile ions, we expect a simple relationship between the conductivity and the phonon lifetime or mode width. Thus the mode broadening is expected to mimic the order parameter. Our results indicate that the order parameter is strongly temperature dependent for this transition; which, as was mentioned above, is not the norm for order-disorder transitions in fast-ion conductors. To first order in the conductivity and ignoring anharmonicity, we write the temperature dependence of the mode width as

$$\gamma=\gamma_0+A\sigma(0)\ .$$

The solid lines in Fig. 7 represent fits to this relationship, where we have used the measured dc conductivity.[2] The excellent results of this analysis reinforces our interpretation of the mode broadening as due to coupling to mobile ions, with a much smaller anharmonicity than that seen in the higher frequency stretching modes.

V. THE PHASE TRANSITION AND THE CONDUCTION MECHANISM

The transition in these materials is unique as it is first order, with a large discontinuity in the ionic conductivity, but does not include a symmetry change (or reconstitution) in the immobile ion sublattice. In many respects the phase transition in these salts is similar to the order-disorder transition in binary alloys such as Cu_3Au.[28] In these systems, however, there are effectively three different entities disordering; the mobile cations (Ag^+ or Cu^+), the Hg^{2+} ions, and the vacancy. Hibma *et al.*[29] have studied the local order in α-Ag_2HgI_4 by diffuse x-ray scattering techniques. They conclude that the most likely situation is that the Hg^{2+} ions are locally ordered over the corners of a cube with the silver ions and vacancies randomly distributed over the face centers. In this model the situation is similar to that of Cu_3Au, with the Hg^{2+} acting as the gold atoms and the Ag ions and the vacancies behaving as the copper atoms. These authors also point out that it is likely that some ions will be considerably displaced from their average positions, by the variations in their local environment.

Girvin and Mahan[30] have constructed a two-component lattice-gas model to describe this phase transition. Since there is no volume change associated with the transition, and the immobile ion sublattice does not change symmetry, it is reasonable to assume it does not participate directly in the phase transition, and therefore this model considers only the cation and vacancy sublattice. The theory correctly predicts the first-order nature of the phase transition; however, since the Hamiltonian does not include a hopping term, it gives no information about the dynamics of the transition. Objections have been raised to this approach by Salamon,[31] who claims a proper accounting of the symmetry of the order parameter has not been made. However, the demonstration that a first-order order-disorder transition can occur in a two-component system allows us to speculate about the dynamics. One possible explanation for the sharpness of the transition is the low mobility of the Hg^{2+} cation and its effect on the mobile cation conduction path. The conduction path for the mobile cations is most likely from the tetrahedral iodine cages through the octahedral cages in the unit-cell center to another tetrahedral cage. In the low-temperature phase the divalent mercury cations occupy a tetrahedral site at one end of the octahedral cage, and it

would be energetically costly for a M^+ cation to enter the octahedral site. The potential seen by the M^+ cations in the tetrahedral cages is fairly flat as demonstrated by the large anharmonicities observed in pressure-dependent Raman studies,[12] and they would be expected to disorder at a lower temperature than the heavier, more tightly bound Hg^{2+} cations. Thus the mercury ions may act as a valve, preventing the mobile cations from disordering by blocking the conduction paths. When the Hg^{2+} ions finally obtain enough energy to surmount their potential barriers, the effective barrier to the motion of the mobile M^+ cations into the octahedral site is reduced. At that temperature there is likely to be a large fraction of the M^+ cations with enough energy to enter the vacant octahedral sites and the disordering will occur rapidly.

Examination of the transition temperatures, activation energies, and ionic radii of the series of silver ternary salts Ag_2YI_4, with Y=Hg, Cd, or Zn, supports this model. As the ionic radius of the Y^{2+} ion increases [Zn, 0.74 Å; Cd, 0.97 Å; and Hg, 1.10 Å (Ref. 32)], the ionic polarizability will also increase. This increased polarizability results in an increased mobility out of the tetrahedral sites, and therefore the temperature at which the silver ions can disorder decreases [for Zn, $T_c=145\,^\circ$C; for Cd, $T_c=80\,^\circ$C; and for Hg, $T_c=50\,^\circ$C (Ref. 33)]. This behavior is also mirrored in the incongruent melting or decomposition temperatures. The activation energy (in the α phase), on the other hand, is a measure of the ability of the silver ions to move through the now disordered lattice. As expected the activation energies [for Zn, $E_A=42$ kJ mol^{-1}; for Cd, $E_A=41$ kJ mol^{-1}; and for Hg, $E_A=36$ kJ mol^{-1} (Refs. 2 and 33)] vary only slightly (15%) among these silver conductors. The decrease in silver-ion activation energy follows the increasing polarizability (and presumed increased mobility) of the Y^{2+} ion.

This two-component disordering is expected to make the phase-transition process depend strongly on the dynamics of the cation-cation and cation-immobile ion interactions. Therefore, any quantitative treatment of this model would have to include details of the local potentials as well as cooperative effects.

ACKNOWLEDGMENTS

We would like to thank Dr. Ryan Dupon for the samples used in this study and for suggesting the incremental application of pressure to avoid decomposition in producing sample pellets. We also thank Professor William Fink for helpful discussion. This work is a portion of the doctoral dissertation of one of us (H.G.L.). The work was supported in part by the Petroleum Research Fund administered by the American Chemical Society.

*Present address: Jet Propulsion Laboratory, California Institute of Technology, Pasadena, CA 91103.

[1]For a general review of the field, see *Fast Ionic Transport in Solids,* proceedings of the International Conference on Fast Ionic Transport in Solids, edited by J. B. Bates and G. C. Farrington (North-Holland, Amsterdam, 1981); *Solid Electrolytes,* edited by S. Geller (Springer, New York, 1977); S. Chadra, *Superionic Solids* (North-Holland, Amsterdam, 1981).

[2]J. A. A. Ketelaar, Z. Kristallogr. **80**, 190 (1931); **87**, 436 (1934), J. A. A. Ketelaar, Phys. Chem. **26B**, 327 (1935); Z. Phys. Chem. **30B**, 53 (1935).

[3]H. Hahn, G. Frank, and W. Klingler, Z. Anorg. Allg. Chem. B279, 271 (1955).

[4]C. E. Olsen and P. M. Harris, Air Force Report No. AFOSR-TN-59-756, 1959 (unpublished).

[5]K. W. Browal, J. S. Kasper, and H. Weidemeier, J. Solid State Chem. **10**, 20 (1974).

[6]A. Miller, A. MacKinnon, and D. Weaire, Solid State Phys. **36**, 119 (1981).

[7]Shuichi Shibata, Hideoki Hoshino, and Mitsuo Shimoji, J. Chem. Soc. (London) Faraday Trans. **70**, 1409 (1974).

[8]David M. Adams and Peter D. Hatton, J. Raman Spectrosc. **14**, 154 (1983).

[9]B. Baranowski, M. Friesel, and A. Lunden, Solid State Ionics **9**, 1179 (1983).

[10]Kazuo Kamigaki, Junichiro Mizuki, and Shunya Abe, Solid State Ionics **3**, 57 (1981).

[11]D. R. Greig, D. F. Shriver, and J. R. Ferraro, J. Chem. Phys. **66**, 5248 (1977).

[12]J. I. McOmber, D. F. Shriver, M. A. Ratner, J. R. Ferraro, and P. LaBonville Walling, J. Chem. Phys. Solids **43**, 903 (1982).

[13]D. R. Greig, G. C. Joy III, and D. F. Shriver, J. Chem. Phys. **67**, 3189 (1977).

[14]J. I. McOmber, D. F. Shriver, and M. A. Ratner, J. Chem. Phys. Solids **43**, 895 (1982).

[15]T. Wong, M. Brodwin, and R. Dupon, Solid State Ionics **5**, 489 (1981).

[16]Platinum Thin Film Thermometers, Omega Engineering Corporation, Stamford, CT 06907.

[17]Artronix Inc., Model No. 5301.

[18]Thermal-Bond 312, Astrodyne, Inc., Hudson, NH 03051.

[19]Infrared Laboratories, Tucson, AZ 85719; similar to N. S. Nishioka, P. L. Richards, and D. P. Woody, Appl. Opt. **17**, 1562 (1978).

[20]H. G. LeDuc, Doctoral dissertation, University of California, Davis, 1983 (unpublished).

[21]See for example, Frederick Wooten, *Optical Properties of Solids* (Academic, New York, 1972).

[22]The oscillator strength is written in several forms, usually as a dimensionless number (f), or in units of frequency squared (S). The two forms are related as $S=f\omega_0^2$.

[23]A detailed discussion of the Kramers-Kronig technique and high-frequency extrapolation schemes can be found in Ref. 21.

[24]T. Wong, M. Brodwin, D. F. Shriver, and J. I. McOmber, Solid State Ionics **3**, 53 (1981).

[25]G. Joy III, Doctoral dissertation, Northwestern University, 1975 (unpublished), as reported by Ref. 14.

[26]M. Peyrard and J. P. Misset, Solid State Commun. **17**, 1487 (1975).

[27]A. Nitzan, M. A. Ratner, and D. F. Shriver, J. Chem. Phys. **72**, 3320 (1980).

[28]See, for example, S. C. Moss, J. Appl. Phys. **35**, 3547 (1964).

[29]T. Hibma, H. U. Beyler, and H. R. Zeller, J. Phys. C **9**, 1691 (1976).

[30]S. M. Girvin and G. D. Mahan, Solid State Commun. **23**, 629 (1977).
[31]M. B. Salamon, in *The Physics of Superionic Conductors,* edited by M. B. Salamon (Springer, New York, 1976).
[32]F. A. Cotton and G. W. Wilkinson, *Advanced Inorganic Chemistry,* 2nd ed. (Wiley-Interscience, New York, 1966), p. 45.
[33]R. L. Ammlong, R. P. Scaringe, J. A. Ibers, D. F. Shriver, and D. H. Whitmore, J. Solid State Chem. **29**, 401 (1979).